Atmos. Meas. Tech., 15, 5455–5464, 2022 https://doi.org/10.5194/amt-15-5455-2022 © Author(s) 2022. This work is distributed under the Creative Commons Attribution 4.0 License.





# Comparison of two photolytic calibration methods for nitrous acid

Andrew J. Lindsay and Ezra C. Wood

Department of Chemistry, Drexel University, Philadelphia, PA, USA

**Correspondence:** Ezra C. Wood (ew456@drexel.edu)

Received: 11 May 2022 - Discussion started: 16 May 2022

Revised: 29 August 2022 – Accepted: 5 September 2022 – Published: 26 September 2022

**Abstract.** Nitrous acid (HONO) plays an important role in tropospheric oxidation chemistry as it is a precursor to the hydroxyl radical (OH). Measurements of HONO have been difficult historically due to instrument interferences and difficulties in sampling and calibration. The traditional calibration method involves generation of HONO by reacting hydrogen chloride vapor with sodium nitrite followed by quantification by various methods (e.g., conversion of HONO to nitric oxide (NO) followed by chemiluminescence detection). Alternatively, HONO can be generated photolytically in the gas phase by reacting NO with OH radicals generated by H<sub>2</sub>O photolysis. In this work, we describe and compare two photolytic HONO calibration methods that were used to calibrate an iodide adduct chemical ionization mass spectrometer (CIMS). Both methods are based on the water vapor photolysis method commonly used for OH and  $HO_2$  (known collectively as  $HO_x$ ) calibrations. The first method is an adaptation of the common chemical actinometry  $HO_x$  calibration method, in which HONO is calculated based on quantified values for [O<sub>3</sub>], [H<sub>2</sub>O], and [O<sub>2</sub>] and the absorption cross sections for  $H_2O$  and  $O_2$  at 184.9 nm. In the second, novel method HONO is prepared in mostly  $N_2$  ( $[O_2] = 0.040\%$ ) and is simply quantified by measuring the NO<sub>2</sub> formed by the reaction of NO with HO<sub>2</sub> generated by H<sub>2</sub>O photolysis. Both calibration methods were used to prepare a wide range of HONO mixing ratios between  $\sim 400$  and 8000 pptv. The uncertainty of the chemical actinometric calibration is 27% ( $2\sigma$ ) and independent of HONO concentration. The uncertainty of the NO<sub>2</sub> proxy calibration is concentration-dependent, limited by the uncertainty of the NO<sub>2</sub> measurements. The NO<sub>2</sub> proxy calibration uncertainties (2 $\sigma$ ) presented here range from 4.5 % to 24.4% (at [HONO] = 8000 pptv and [HONO] = 630 pptv,

respectively) with a 10 % uncertainty associated with a mixing ratio of  $\sim$  1600 pptv, typical of values observed in urban areas at night. We also describe the potential application of the NO<sub>2</sub> proxy method to calibrating HO<sub>x</sub> instruments (e.g., LIF, CIMS) at uncertainties below 15 % (2 $\sigma$ ).

## 1 Introduction

Nitrous acid (HONO) is a source of the most important atmospheric oxidant – the hydroxyl radical (OH) – and can therefore play an important role in tropospheric oxidation chemistry. The hydroxyl radical initiates the removal of most trace gases from the atmosphere, leading to the formation of secondary pollutants such as ozone  $(O_3)$  and secondary aerosols. Photolysis of HONO yields OH and nitric oxide (NO):

$$HONO + hv \rightarrow OH + NO (\lambda < 400 \text{ nm}).$$
 (R1)

This reaction is the primary sink of HONO during the daytime, leading to a typical chemical lifetime at mid-day of between 10–20 min at mid-latitudes. Sources of HONO include homogeneous formation (Reaction R2), direct emissions from combustion (vehicles, biomass burning, etc.) and soils, and numerous heterogenous processes including heterogeneous reaction of NO<sub>2</sub> with moist terrestrial surfaces, photolysis of particulate nitrate (Ye et al., 2016, 2017), and photolysis of nitric acid (Ye et al., 2016).

$$OH + NO + M \rightarrow HONO + M$$
 (R2)

The relative importance of these sources varies with environment (Jiang et al., 2022).

HONO photolysis has been reported as a major source of  $HO_x$  ( $HO_x = OH + HO_2$ ) throughout the day in a variety

of environments, including urban and highly polluted areas (Whalley et al., 2018; Slater et al., 2020; Ren et al., 2013; Lu et al., 2019) as well as more pristine environments (Villena et al., 2011; Jiang et al., 2020; Bloss et al., 2007). Vertical distributions of HONO, however, indicate that its significance as a  $HO_x$  precursor may be limited to near ground level (Li et al., 2014; Young et al., 2012; Villena et al., 2011; Wong et al., 2012; Tuite et al., 2021; Jaeglé et al., 2018). HONO can also serve as an important source of  $HO_x$  in indoor environments since sufficient UV light can penetrate windows, and substantial HONO concentrations can result from various activities (e.g., cooking) (Gomez Alvarez et al., 2013; Wang et al., 2020).

HONO is notoriously difficult to measure. It can be formed via heterogeneous chemistry within sampling lines or an instrument's inlet. The resulting interferences may pose additional challenges in applying an instrument's zero or in calibration processes that alter the interfering species. Some intercomparison studies have shown substantial differences between HONO measurement techniques. A comparison of several HONO measurements in Beijing showed an overall mixed agreement with a few instruments disagreeing by more than a factor of 2 (Crilley et al., 2019). Measurements in Houston, Texas, showed overall good agreement (within 20%) between most instruments, with larger differences of over 100% observed for one of the instruments for some time periods (Pinto et al., 2014). Bourgeois et al. (2022) recently reported an 80 % difference between HONO measurements made by cavity-enhanced spectroscopy and iodide-adduct chemical ionization mass spectrometry (CIMS). Closer agreement for two instrument comparisons has been reported by Stutz et al. (2010; comparing differential optical absorption spectroscopy (DOAS) and mist-chamber ion chromatography (IC)), Cheng et al. (2013; comparing long-path absorption photometry (LOPAP) and stripping coil IC), and Dixneuf et al. (2022; comparing LOPAP and cavity-enhanced absorption spectroscopy), though many of these studies report considerable deviations when HONO mixing ratios were less than  $\sim 100$  pptv.

Calibrations for HONO are challenging as this compound is not commercially available and rather must be prepared in situ. Most commonly, HONO is prepared by reacting hydrogen chloride vapor with sodium nitrite (Febo et al., 1995):

$$HCl_{(g)} + NaNO_{2(s)} \rightarrow HONO_{(g)} + NaCl_{(s)}.$$
 (R3)

This method presents several challenges. A stable source of HCl is required, usually from a heated aqueous solution, a gas cylinder, or a permeation tube. Consistent mixing between the HCl and the NaNO<sub>2</sub> powder is required. These calibrations also require substantial warmup times (often hours) to ensure source stability, though some recent versions report faster warmup periods (e.g., < 10 min reported by Villena and Kleffmann, 2022). High HONO concentrations (above 1 ppmv) are often produced, requiring dilution, though the temporary unrealistic HONO concentrations can

lead to significant HONO loss by its self-reaction and inaccurate HONO quantification. A recent, noteworthy version of this calibration improves upon this concentration issue and has the ability to produce [HONO] on the order of tens of parts per trillion by volume (Lao et al., 2020). The generated HONO can be quantified by various methods including theoretical calculation (Villena and Kleffmann, 2022), conversion to NO followed by chemiluminescence detection (Lee et al., 2012; Lao et al., 2020; Villena and Kleffmann, 2022), thermal conversion to NO<sub>2</sub> followed by NO<sub>2</sub> quantification (Gingerysty and Osthoff, 2020), and conversion to aqueous nitrite followed by derivatization and detection by UV-vis (Peng et al., 2020). The calibration uncertainty depends on the output stability of the HONO source and the quantification technique used. Villena and Kleffmann (2022) demonstrate using two separate techniques that overall calibration uncertainties can be well below 10% ( $2\sigma$ ).

More recently, photolytic HONO sources have been utilized. Humidified air is exposed to ultraviolet (UV) light to photolyze H<sub>2</sub>O to produce an equal mixture of OH and HO<sub>2</sub>, which in the presence of excess NO then converts to HONO. This HONO output is stable within seconds (i.e., the initial UV lamp warmup time) and is tunable by altering humidity, UV flux, or UV exposure time. The HONO formed has been quantified based on the water vapor mixing ratio, water vapor absorption cross section, UV flux, and UV exposure time. This quantification approach thus far has been used to calibrate photo-fragmentation LIF instruments (Dyson et al., 2021; Bottorff et al., 2021). The HONO formed from a photolytic source has also been quantified by thermal dissociation followed by measurement of the NO2 produced (Veres et al., 2015). These methods have an uncertainty of 30 % to 36 % (2 $\sigma$ ), similar to the uncertainty for HO<sub>x</sub> calibrations based on water vapor photolysis (Dusanter et al., 2008). In this paper, we present an alternative photolytic HONO calibration that we refer to as the "NO2 proxy" method. This method requires a direct NO<sub>2</sub> measurement that is used as a "proxy" to quantify HONO concentrations. We compare this new proxy calibration to the more standard photolytic calibration method as performed by Bottorff et al. (2021) and Dyson et al. (2021). This method has a lower uncertainty (typically  $\sim 10\%$ ,  $2\sigma$ ) and unlike the actinometric method does not require characterization of the mercury lamp emission spectrum.

#### 2 Methods

#### 2.1 Instrumentation

A cavity attenuated phase shift (CAPS) spectrometer (Aerodyne Research, Inc.) was used to detect NO<sub>2</sub> (Kebabian et al., 2008). The CAPS also indirectly measured O<sub>3</sub> as it was converted to NO<sub>2</sub> by reaction with excess NO. The CAPS instrument was calibrated using a 2B Technologies

model 306 O<sub>3</sub> calibration source. Ozone outputs were varied between 10 and 300 ppbv with greater than 99.99 % conversion efficiency to NO<sub>2</sub> by reaction with excess NO ([NO] = 1.82 ppmv) within approximately 15 m of FEP tubing (i.d. = 0.476 cm; residence time = 17.1 s, pseudo-first order rate constant of 0.8 s<sup>-1</sup>). The manufacturer-stated accuracy of this  $O_3$  calibrator is 2% (2 $\sigma$ ), though no recent factory calibrations have been conducted. Therefore, a second calibration was conducted with a Thermo Environmental Instruments 49C O<sub>3</sub> calibrator, which agreed to within 2.5 %. We assign an uncertainty of 4 %  $(2\sigma)$  to the NO<sub>2</sub> measurements to account for possible drift in accuracy. Temperature and relative humidity (RH) measurements were made using two Vaisala HMP60 probes and used, along with pressure measurements, to calculate  $H_2O_{(g)}$  mixing ratios. Both probes agreed with a new RH-T replacement sensor (manufacturer-stated uncertainty: 3 %) to within 3 %. We assign an uncertainty of 5 %  $(2\sigma)$  to our determined H<sub>2</sub>O mixing ratios.

A high-resolution chemical ionization time-of-flight mass spectrometer (HR-ToF-CIMS, Tofwerks/Aerodyne Research, Inc.) was used to detect HONO (Bertram et al., 2011; Lee et al., 2014). HONO and concomitant gases are ionized within a laboratory-built ion-molecule reactor (IMR) using reagent iodide (I<sup>-</sup>) ions. Our lab-built IMR is internally coated with PTFE and sampled the calibration gas at a flow rate of 2.10 slpm through a stainless-steel critical orifice (nominal diameter of 0.48 mm). Iodide (I<sup>-</sup>) reagent ions in N2 (Airgas, industrial grade) were sampled at 2.20 slpm through a similar critical orifice perpendicular to the main sample flow. The I<sup>-</sup> was prepared by exposing dilute methyl iodide (CH<sub>3</sub>I) from a permeation tube (VICI Metronics) to a <sup>210</sup>Po radioactive source. Humidified N<sub>2</sub> was also added to the IMR perpendicular to the main sample flow at a flow rate of 0.365 slpm. The pressure in the IMR was held at 80 mbar, controlled by adjusting a valve to a scroll pump (Agilent Technologies IDP-7).

Ions are separated by mass-to-charge ratio (m/z) at a mass resolving power of near  $5000 \,\mathrm{m} \,\Delta\mathrm{m}^{-1}$ . We monitor the HONO iodide adduct I(HONO)<sup>-</sup> at  $173.90575 \, m/z$ . The peak-fitting software (TofWare) accounts for the overlapping contribution from the  $^{13}\mathrm{C}$  formic acid I( $^{13}\mathrm{CH}_2\mathrm{O}_2$ )<sup>-</sup> peak at  $173.91342 \, m/z$ . We account for the humidity dependence of the instrumental response by determining the mole fraction of  $\mathrm{H}_2\mathrm{O}_{(g)}$  ( $\chi_{\mathrm{H}_2\mathrm{O}}$ ) in the IMR by measuring the RH and temperature of the IMR in the exhaust of the scroll pump. See the Supplement for more information regarding humidity effects for the HONO ionization chemistry (see Sect. S1.2). Analytical parameters including the limit of detection, precision, and linear range of these HONO measurements are also detailed within the supplement (see Sect. S1.1).

#### 2.2 Calibration methods

We calibrate HONO using two variations of the water vapor HO<sub>x</sub> calibration method: one is a modification of the standard actinometric  $HO_x$  photolytic calibration, and the other we refer to as the "NO<sub>2</sub> proxy" calibration. These calibration methods mainly differ in how HONO is quantified. In both methods, HONO was produced nearly identically. Air (Airgas, Ultra Zero grade;  $[O_2] = 21 \pm 1 \%$ ) for the actinometric method or N<sub>2</sub> (Airgas, industrial grade) for the NO<sub>2</sub> proxy calibration is humidified with HPLC (high-performance liquid chromatography) grade water (Fisher Chemical), mixed with NO (Airgas,  $41.02 \pm 2.05$  ppmv in N<sub>2</sub>), and then exposed to 184.9 nm ultraviolet radiation from a low-pressure mercury lamp (Jelight 78-2046-1). While in the experiments presented in this paper we used industrial grade N<sub>2</sub> for the humidified CIMS IMR inflow (mentioned in Sect. 2.1) and as the NO<sub>2</sub> proxy calibration carrier gas, we have used ultrahigh-purity N<sub>2</sub> (Airgas) in previous experiments. We find no differences between the calibration results acquired using different grades of N2. The resulting OH and HO2 from water photolysis form HONO by reaction with excess NO (Reactions R4-R6a and R2).

$$H_2O + hv \rightarrow H + OH$$
 (R4)

$$H + O_2 + M \rightarrow HO_2 + M \tag{R5}$$

$$HO_2 + NO \rightarrow OH + NO_2$$
 (R6a)

$$OH + NO + M \rightarrow HONO + M$$
 (R2)

The HO<sub>2</sub>-to-HONO pathway is limited by the small fraction of Reaction (R6) that forms HNO<sub>3</sub> rather than OH and NO<sub>2</sub>:

$$HO_2 + NO + M \rightarrow HNO_3 + M.$$
 (R6b)

A schematic of the setup used for both calibrations is shown in Fig. 1. The mercury lamp is housed within a  $10.8 \,\mathrm{cm} \times 26.7 \,\mathrm{cm} \times 10.2 \,\mathrm{cm}$  photolysis chamber (Fig. 1b), and the volume surrounding the lamp is purged with dry N<sub>2</sub> (purge not shown). The humidified air–NO mixture is transported past the mercury lamp within a partially exposed quartz tube (I.D. = 1.04 cm, total length = 26.7 cm; exposed length  $= \sim 0.5$  cm). HONO sample concentrations are controlled by adjusting the lamp flux with a Variac variable transformer, adjusting the relative flow rates of the dry and humidified zero air–N<sub>2</sub>, or adjusting the absolute flow rates to alter the lamp exposure time. For our example calibrations discussed in this paper, we typically used a main N<sub>2</sub> or air flow rate of 5 slpm with an addition of 200 sccm of 41.02 ppmv NO in N<sub>2</sub> for a total flow rate of 5.20 slpm and a diluted NO mixing ratio of 1.58 ppmv. Pseudo-first-order rate constants calculated using this [NO] for Reactions (R6a) and (R2) are 322 and 295 s<sup>-1</sup>, respectively. Under these conditions,  $HO_x$  is converted to HONO within 0.02 s inside the remaining 11.4 cm of the quartz tube. The [NO] chosen must be high enough to minimize OH and HO<sub>2</sub> wall losses. We have ensured that this NO mixing ratio is sufficient in separate experiments by confirming that no additional HONO signal results at increased [NO] values. Possible HONO formation by additional photolytic processes (specifically involving the surfaces of the quartz photolysis tube) was tested by monitoring CIMS I(HONO) signals during additional experiments. These experiments include exposing dry carrier gas ([NO] = 1.58 ppmv) to 184.9 nm radiation (i.e., exposure to UV without H<sub>2</sub>O photolysis), exposing humidified carrier gas ([NO] = 0 ppmv) to 184.9 nm radiation (i.e., to investigate if HONO is formed by heterogenous reactions involving H<sub>2</sub>O or HO<sub>x</sub> with NO, NO<sub>2</sub>, or HNO<sub>3</sub> adsorbed on the quartz tube), and exposing humidified carrier gas ([NO] = 1.58 ppmv) to the 254 nm radiation from a separate mercury lamp (Jelight 81-3306-2) in which the 184.9 nm emission is blocked (i.e., the carrier gas matches calibration conditions and is exposed to UV radiation but without H2O photolysis). These tests indicate no appreciable HONO formation by other photolytic processes.

The resulting calibration gas enters a PFA tee and is arranged so that the air travels straight to the CIMS (2.1 slpm) while the remaining flow ( $\sim 3.1 \text{ slpm}$ ) makes a 90° turn for the CAPS line, which includes a vent. The gas flow is initially laminar within the quartz photolysis tube (Reynolds number  $\approx$  600). This results in an initial [HO<sub>2</sub>] (and therefore [HONO]) radial gradient in which the greatest concentrations exist near the flow tube walls (i.e., where the flow rates are lower and the UV exposure times longer). Turbulence is induced by the sudden changes in tube inner diameter at the quartz tube exit (reducing union) and upon entering the PFA tee. The air is therefore most likely well mixed prior to being split within the PFA tee. The excess flow within the CAPS line ( $\sim 2 \text{ slpm}$ ) was vented past an RH-T probe to determine the water mixing ratio in the photolysis cell. A second RH-T probe quantified the water mixing ratio in the CIMS IMR as previously mentioned in Sect. 2.1. Details of the two calibration methods are described in the following sections.

# 2.2.1 Actinometric calibration

The water vapor photolysis calibration method has been used for several decades to calibrate OH and  $HO_2$  measurements (Stevens et al., 1994; Lanzendorf et al., 1997; Dusanter et al., 2008). The concentration of  $HO_x$ , and therefore HONO, is calculated from the time-integrated photolysis of water vapor:

$$[HONO] \approx [HO_x] = (F \cdot t)[H_2O]\sigma_{H_2O}\Phi_{HO_x}, \tag{1}$$

where F is the photon flux at 184.9 nm, t is the UV irradiation time,  $\sigma_{\rm H_2O}$  is the absorption cross section of water at 184.9 nm, and  $\Phi_{\rm HO_x}$  is the quantum yield of  ${\rm HO_x}$  from water photolysis and equal to 2. F can be quantified using direct actinometric measurements (e.g., using a calibrated phototube), and t can be quantified via characterization of the flow

rates and photolysis cell geometry (Faloona et al., 2004). Alternatively, and more commonly among  $HO_x$  measurement groups, the product  $F \cdot t$  can be determined via "chemical actinometry" (Schultz et al., 1995). In the  $O_2$ – $O_3$  chemical actinometry method, the concentration of  $O_3$  produced by photodissociation of  $O_2$  at 184.9 is used to determine  $F \cdot t$ :

$$O_2 + hv \rightarrow O + O,$$
 (R7)

$$O + O_2 + M \rightarrow O_3 + M. \tag{R8}$$

The product of the lamp flux and the exposure time, i.e., the  $(F \cdot t)$  term, is given by Eq. (2), in which  $\sigma_{O_2}$  is the absorption cross section of  $O_2$  at 184.9 nm and  $\Phi_{O_3}$  is quantum yield of  $O_3$  from  $O_2$  photolysis ( $\Phi_{O_3} = 2$ ):

$$(F \cdot t) = \frac{[O_3]}{[O_2] \sigma_{O_2} \Phi_{O_3}}.$$
 (2)

Substituting this expression for  $F \cdot t$  into Eq. (1) gives Eq. (3):

[HONO] 
$$\approx$$
 [HO<sub>x</sub>] =  $\frac{[O_3]}{[O_2]\sigma_{O_2}}$  [H<sub>2</sub>O]  $\sigma_{H_2O}$ . (3)

The effective value for  $\sigma_{O_2}$  must be experimentally determined for the individual mercury lamp at the experimental O<sub>2</sub> optical depth. This is required because the emission profile near 184.9 nm, which comprises two peaks due to self-reversal, can vary from lamp to lamp and with operating conditions, and the O2 absorption spectrum steeply decreases near the mercury lamp emission maximum (Lanzendorf et al., 1997). We use an experimentally determined  $\sigma_{\rm O_2}$  value of  $1.4 \times 10^{-20}$  cm<sup>2</sup> molec.<sup>-1</sup> for the mercury lamp used for these experiments. The JPL-recommended value of  $7.1 \times 10^{-20} \, \text{cm}^2$  molec.<sup>-1</sup> was used for  $\sigma_{\text{H}_2\text{O}}$  (Burkholder et al., 2020). The value of [O<sub>2</sub>] is based on the flows mentioned in Sect. 2.2 and is equal to  $20.1\pm1.0$  %. The O<sub>2</sub> optical depth is 0.033, and the O<sub>2</sub> column density (within the photolysis tube center) is  $2.4 \times 10^{18}$  molec. cm<sup>-2</sup>. For typical operating conditions, the value of  $F \cdot t$  and an estimated photon flux F (calculated using an approximate gas exposure time) are  $3.48 \times 10^{12}$  photons cm<sup>-2</sup> and  $7.1 \times 10^{14}$  photons cm<sup>-2</sup> s<sup>-1</sup>, respectively. The value of [O<sub>3</sub>] here was near 20 ppbv and determined with the CAPS NO<sub>2</sub> monitor after its reaction with NO, forming NO<sub>2</sub>. This is measured with dry air flowing in the photolysis chamber so that the NO<sub>2</sub> measured is solely from the reaction of NO with  $O_3$  and not  $HO_2$ . These  $F \cdot t$ and [O<sub>3</sub>] values are high compared to those used for most  $O_3$  actinometry  $HO_x$  calibrations, in which  $[O_3]$  is often less than 1 ppbv (e.g., Faloona et al., 2004), but are comparable to those used by Dusanter et al. (2008). High  $F \cdot t$  values were used so that typical ambient HONO concentrations (ranging up to several parts per billion by volume) could be prepared. [H<sub>2</sub>O] is determined using the measured RH, temperature, and pressure. The uncertainties of the variables in Eq. (3) are discussed in Sect. S3. The combined uncertainty  $(2\sigma)$  for  $[HO_x]$  (and therefore [HONO]) calculated using this equation is 27 % (see Supplement for details).

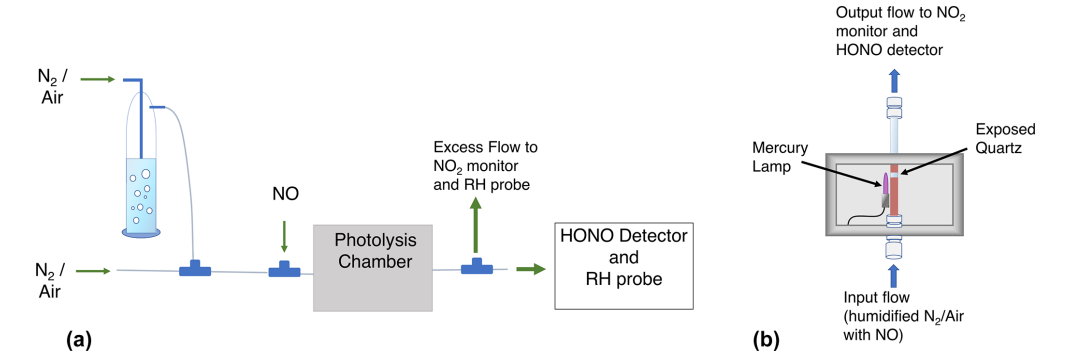


Figure 1. Schematic of the experimental setup (a) and the photolysis chamber (b). Not shown: small flow of air when using  $N_2$  as the carrier gas (a) and the purge flow of  $N_2$  (b).

We apply a small correction to the value for  $[HO_x]$  calculated in Eq. (3) in order to obtain [HONO]. This correction accounts for the incomplete conversion of  $HO_2$  to HONO due to Reaction (R6b).

$$[HONO] = \left(0.5 + 0.5 \cdot \frac{1}{1+\beta}\right) \cdot [HO_x] \tag{4}$$

Equation (4) includes the variable  $\beta$ , which is the relative rate or product ratio of Reaction (R6b) to (R6a) (i.e.,  $\beta = k_{\rm R6b}/k_{\rm R6a} = [{\rm HNO_3}]/[{\rm NO_2}]$ ) and depends on temperature, pressure, and humidity (Butkovskaya et al., 2007, 2009). The term  $(1/(1+\beta)$  in Eq. (4) represents a traditional branching ratio (i.e.,  $k_{\rm R6b}/(k_{\rm R6a}+k_{\rm R6b})=[{\rm HNO_3}]/([{\rm NO_2}]+[{\rm HNO_3}])$ ). For the experiments conducted, the value of  $\beta$  is at most 0.04, leading to a 2% correction to Eq. (1). See Sect. S2 for information regarding the formulation of Eq. (4) and the calculation of  $\beta$ .

The CIMS response to HONO is determined by acquiring a background by briefly toggling off the mercury lamp. This background CIMS signal is humidity dependent, so a background is taken at each humidity setting. Background CIMS I(HONO)<sup>-</sup> signals are elevated during calibrations due to impurities in the NO flow.

#### 2.2.2 Proxy calibration

For the NO<sub>2</sub> proxy calibration method, we determine [HONO] from the measured value of [NO<sub>2</sub>] formed from Reaction (R6a) during HONO production. For each H<sub>2</sub>O molecule photolyzed (Reaction R4), nearly one NO<sub>2</sub> and two HONO molecules are produced. Therefore, [HONO] is simply given by the measured [NO<sub>2</sub>] (Eq. 5):

$$[HONO] = (2 + \beta) \cdot [NO_2], \tag{5}$$

where  $\beta$  is added to account for the minor HNO<sub>3</sub> product of the HO<sub>2</sub>+ NO reaction (Reaction R6b).

For the proxy calibration we use humidified  $N_2$  rather than air and include a small addition of 10 sccm of zero air prior to lamp exposure (not shown in the Fig. 1 schematic). The

resulting low  $O_2$  concentration ( $[O_2] = 0.040 \pm 0.002 \%$ ) is sufficient for the full conversion of H to HO<sub>2</sub> (Reaction R5) but results in a negligible amount of O<sub>3</sub> formed by O<sub>2</sub> photolysis (Reactions R7–R8), confirmed by toggling the UV source on and off with dry carrier gas flowing. The pseudofirst-order rate constant for the H to HO<sub>2</sub> conversion (Reaction R5) is  $1.1 \times 10^4$  s<sup>-1</sup> for this [O<sub>2</sub>] value. HONO concentrations are quantified using background subtracted [NO2] values in Eq. (5), which are typically acquired by toggling the mercury lamp off and on. The CIMS signal response is determined simultaneously. A "direct" NO2 detection method is highly recommended over indirect methods that rely on NO detection as the high NO mixing ratios would result in degraded precision. For this study we used a CAPS instrument, but other methods like cavity ring-down spectroscopy (CRDS), laser-induced fluorescence (LIF), or oxygen anion CIMS (e.g., Novak et al., 2020) would be acceptable.

## 3 Results and discussion

Time series data for the proxy calibration method are shown in Fig. 2. The CAPS NO<sub>2</sub> measurement and the CIMS HONO signal normalized to 1 million counts per second of reagent ion ("ncps") are shown at a constant humidity (RH = 29%,  $\chi_{H_2O} = 0.0065$ , T = 19.3 °C, P = 760 Torr within the photolysis cell and RH = 19 \%,  $\chi_{H_2O} = 0.0042$ , T = 19.2 °C, P = 760 Torr within the CIMS IMR exhaust). The NO<sub>2</sub> data are shown with an offset so that concentrations are near 0 ppbv while the UV source is off. Background [NO<sub>2</sub>] values were typically near 15 ppbv due to impurities within the NO cylinder and NO<sub>2</sub> production from the termolecular reaction NO + NO + O<sub>2</sub>  $\rightarrow$  2 NO<sub>2</sub>. During the first 120 s shown in Fig. 2, HONO is formed by H<sub>2</sub>O photolysis via the mercury lamp 184.9 nm emission. This leads to the stable I(HONO) signal in the CIMS along with enhanced [NO<sub>2</sub>] produced by Reaction (R6a) and measured by the CAPS monitor. Background I(HONO)<sup>-</sup> and NO<sub>2</sub> signals are determined by toggling off the mercury lamp (shown at 121 s). The CIMS sensitivity (ncps ppt $^{-1}$ ) is equal to the quo-

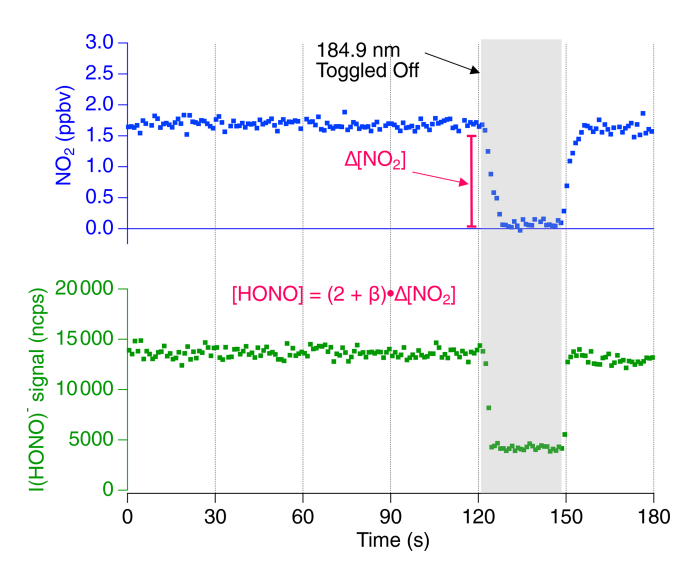


**Figure 2.** The 1 s averaged time series data for a proxy calibration at a constant relative humidity. The iodide HONO adduct signal (cps) is shown normalized per 1 million reagent ions (ncps). The shaded section represents the period in which the 184.9 nm mercury lamp is toggled off to obtain background [NO<sub>2</sub>] and HONO signal. The NO<sub>2</sub> concentration is shown with an offset so that background values are near 0 ppbv. The resulting difference in NO<sub>2</sub> indicates that approximately 3000 pptv [HONO] is sampled by the CIMS.

tient of the normalized background subtracted CIMS signal and the quantified [HONO] which is calculated by Eq. (5).

A multipoint NO<sub>2</sub> proxy calibration curve (Fig. 3) shows the linear CIMS signal response to [HONO]. This calibration was conducted at a constant relative humidity (RH = 28 %,  $\chi_{\rm H_2O} = 6.22 \times 10^{-3}$ ,  $T = 19.3 \,^{\circ}$ C,  $P = 760 \,^{\circ}$ Torr within the photolysis cell and RH = 18 %,  $\chi_{H_2O} = 3.88 \times 10^{-3}$ , T =19.2 °C, P = 760 Torr within the CIMS IMR exhaust), and [HONO] was adjusted by altering the mercury lamp flux with a Variac variable transformer. The slope of this curve,  $2.89 \pm$  $0.34 \,\mathrm{ncps}\,\mathrm{ppt}^{-1}$  (2 $\sigma$ ), is the CIMS sensitivity to HONO for this particular water mole fraction within the CIMS IMR  $(\chi_{\rm H_2O} = 3.88 \times 10^{-3})$ . HONO mixing ratios ranged from approximately 400 to 3500 pptv, thus demonstrating that a wide range in HONO concentrations can easily be prepared. The uncertainties for the quantified [HONO] values from Eq. (5) (i.e., the x-error bars) are obtained by adding in quadrature three terms: (1) the relative uncertainty of the NO<sub>2</sub> background subtraction (based on the 5s average precision of 27 pptv), (2) the NO<sub>2</sub> calibration uncertainty (3 \%, 2 $\sigma$ ), and finally (3) the relative uncertainty associated with the  $(2+\beta)$ expression (typically 0.14 %,  $2\sigma$ ). The uncertainty in the normalized CIMS signal is obtained by adding in quadrature the 15 s precision of the I(HONO) signal with that of the reagent ion. The  $2\sigma$  error bars range from 6.1 % to 34.8 % for quantified [HONO] and 1.7 % to 2.9 % in the CIMS HONO signal. The Fig. 3 slope (i.e., the CIMS sensitivity to HONO) and its uncertainty were determined using the York bivariate

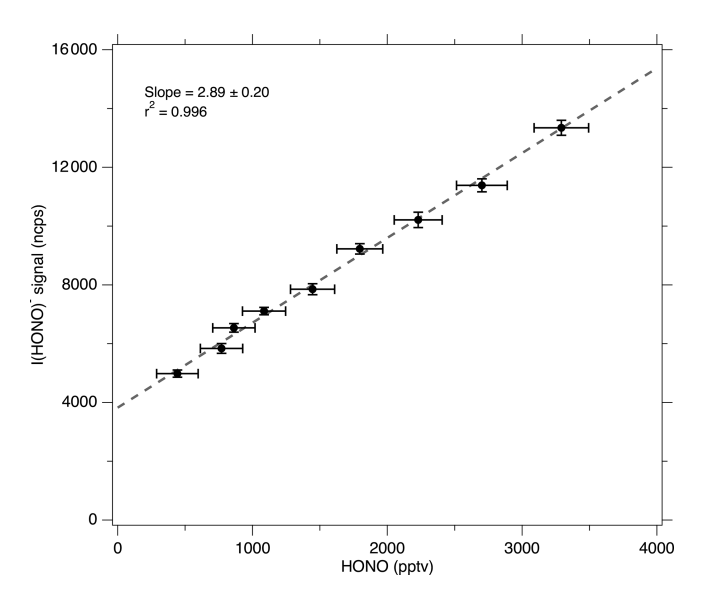


**Figure 3.** Calibration curve obtained using the NO<sub>2</sub> proxy calibration method at a constant humidity (RH = 17.7 %, [H<sub>2</sub>O] = 0.388 % as measured in the CIMS scroll pump exhaust) by varying photon flux F with a Variac variable transformer. Error bars represent  $\pm 2\sigma$  uncertainty. The data were fitted using the York bivariate regression method (York et al., 2004). The y intercept (3820 ncps) represents the background CIMS I(HONO)<sup>-</sup> signal during this calibration and is mostly from impurities in the constant NO addition. Without the NO addition (for ambient sampling), the typical background signal is 75 ncps.

linear regression method (York et al., 2004). The uncertainty calculations are discussed in greater detail in Sect. S4.1.

A comparison between the more standard O<sub>3</sub> actinometrybased calibration and the new proxy calibration method is shown in Fig. 4. CIMS sensitivities as determined by single point calibrations are shown for a variety of  $\chi_{H_2O}$  values. The two calibration methods were conducted consecutively and agree within their respective  $2\sigma$  uncertainties. Sensitivities ranged from 1.5 to 5.3 ncps  $ppt^{-1}$  with the greatest values observed at low- $\chi_{H_2O}$  settings. The CIMS IMR  $\chi_{H_2O}$ values ranged from  $1.77 \times 10^{-3}$  to  $8.25 \times 10^{-3}$  and corresponded to a photolysis cell RH range of 4.1 % to 71 % and photolysis cell  $\chi_{\rm H_2O}$  values of  $0.93 \times 10^{-3}$  to  $16 \times 10^{-3}$  (average T = 19.6 °C; P = 760 Torr). The sensitivity determined by the Fig. 3 multipoint calibration  $(2.89 \pm 0.34 \,\mathrm{ncps}\,\mathrm{ppt}^{-1})$ at CIMS IMR  $\chi_{\rm H_2O} = 3.88 \times 10^{-3}$ ) is consistent with those shown in Fig. 4 at similar  $\chi_{H_2O}$  values. These CIMS sensitivities are also in line with literature values (Peng et al., 2020; Bourgeois et al., 2022). Unique to this figure is the use of the CIMS IMR  $\chi_{H_2O}$  to track humidity dependence rather than the partial pressure of H<sub>2</sub>O (Lee et al., 2014), the specific humidity (Novak et al., 2020), or the CIMS signal ratio of the iodide water adduct  $I(H_2O)^-$  (m/z 145) to reagent ion  $I^{-}$  (m/z 127; Lee et al., 2014; Peng et al., 2020; Veres et al., 2015, 2020). The use of  $\chi_{H_2O}$  allows for a more direct comparison to other CIMS instruments that may use differ-

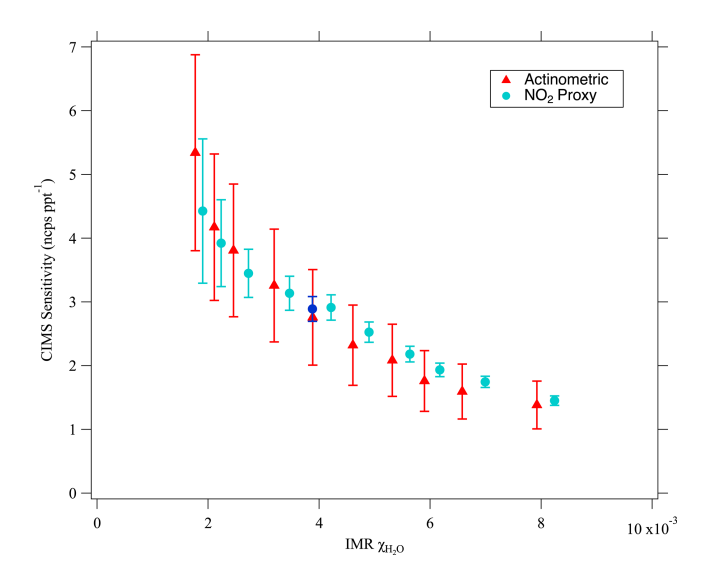


**Figure 4.** Comparison of the two HONO calibration methods for a range of  $\chi_{\rm H_2O}$  within the CIMS IMR. The sensitivity determined by the multipoint calibration (i.e., the Fig. 3 slope) is plotted as the dark blue circle. Error bars represent  $\pm 2\sigma$  uncertainties. [HONO] ranged from 470 pptv (at the lowest  $\chi_{\rm H_2O}$  value) to 7710 pptv (at the greatest  $\chi_{\rm H_2O}$  value) for the actinometric calibration. [HONO] similarly ranged from 630 to 7820 pptv for the NO<sub>2</sub> proxy calibration.

ent IMR pressures and quadrupole voltage settings that govern the ratio of  $I(H_2O)^-$  to  $I^-$ . See the supplement for more information regarding humidity effects on ionization chemistry (Sect. S1.2).

The uncertainty in the CIMS sensitivity for the singlepoint proxy calibration points in Fig. 4 is determined by combining in quadrature the relative uncertainty of the background subtracted CIMS signal with that of the quantified [HONO] value. The calculation for quantified [HONO] uncertainty and CIMS uncertainty is previously mentioned in the text regarding Fig. 3, though the CIMS uncertainty here slightly differs due to the background subtraction (see Sect. S4.2). As mentioned previously, the total uncertainty depends on the quantified [HONO] value, which ranged from 630 (at the lowest  $\chi_{H_2O}$  value) to 7800 pptv (at the greatest  $\chi_{H_2O}$  value) for the proxy calibration results shown in Fig. 4. The uncertainty for the greatest [HONO] values (corresponding to the highest  $\chi_{H_2O}$  settings) is dominated by the  $4\% 2\sigma$  accuracy of the  $NO_2$  measurement. At the lowest [HONO] values (shown at lowest  $\chi_{H_2O}$  settings), larger uncertainties occur and are dominated by the precision in NO<sub>2</sub> measurements due to the background subtraction. Therefore, the uncertainty can be minimized by using higher HONO concentrations. The presented  $2\sigma$  uncertainty in sensitivity using the proxy method ranged from 5.1 % to 25.5 % with the [HONO] quantification alone accounting (from Eq. 4) for 4.5 % to 24.4 %. These proxy calibration uncertainties for [HONO] fall well below the 27 %  $2\sigma$  uncertainty associated with the standard  $O_3$  actinometry calibration. The  $2\sigma$  uncertainty in sensitivities determined by our actinometry calibrations (i.e., the 27% method uncertainty combined with precision of the CIMS measurement) varies from 27.1% to 28.8%. The proxy calibration therefore allows for lower uncertainties compared to the standard actinometry calibration, especially at high [HONO] values.

## 4 Application to $HO_x$ calibrations

In addition to its use described herein for HONO calibrations, the  $NO_2$  proxy method can also be used to determine the prepared  $HO_x$  concentration (i.e., prior to its reaction with NO), which differs from [HONO] by only a few percent depending on the value of  $\beta$ .

$$[HO_x] = (2+2\beta) \cdot [NO_2] \tag{6}$$

Directly using this method to calibrate a  $HO_x$  instrument (e.g., LIF,  $HO_x$ -CIMS, or perCIMS) is likely not feasible as the described calibration is performed in  $N_2$  rather than air (i.e., the composition of the calibration carrier gas should be identical to that for ambient air) and requires high NO mixing ratios that could complicate the operation of a  $HO_x$  instrument more than it does for our iodide CIMS.

The application of an NO<sub>2</sub> proxy calibration for a HO<sub>x</sub> instrument would likely require two consecutive steps. First an NO<sub>2</sub> proxy calibration would be performed as described in this paper (with high [N<sub>2</sub>], high [NO], and only the NO<sub>2</sub> instrument sampling). Second, the N<sub>2</sub> and NO flows would be replaced with zero air, and the resulting calibration mixture, which would have the same HO<sub>x</sub> concentration as determined by the NO<sub>2</sub> proxy calibration, would then be sampled by a HO<sub>x</sub> instrument. Additional concentrations of HO<sub>x</sub> could be prepared by altering and tracking [H<sub>2</sub>O]:

$$[HO_x] = \frac{[HO_x]_{proxy}}{[H_2O]_{proxy}} [H_2O], \tag{7}$$

where the "proxy" designation refers to the corresponding values of [HO $_x$ ] (quantified via Eq. 6) and [H $_2$ O] during the proxy calibration step (i.e., high [NO] and N $_2$  as the carrier gas). The quotient of [HO $_x$ ] and [H $_2$ O] is equal to the product of the constants  $F \cdot t \cdot \sigma_{H_2O} \cdot \Phi_{HO_x}$  that appear in Eq. (1).

The uncertainty in  $[HO_x]$  will likely range 5% to 15%  $(2\sigma)$ , similar to that for [HONO] quantified via proxy calibration, mainly dependent on the  $[NO_2]$  measurement uncertainty. While the accuracy in  $H_2O$  measurements should not contribute to the Eq. (7)  $[HO_x]$  uncertainty as it effectively cancels out, the precision in the  $[H_2O]$  measurements would have to be accounted for. The uncertainty for this proposed method is exceptional compared to typical  $HO_x$  calibrations in which total uncertainties are often above 25%  $(2\sigma)$  based on the combination of Eq. (1) parameters of  $F \cdot t$ ,  $\sigma_{H_2O}$ , and  $[H_2O]$ .

## 5 Conclusions

Two photolytic HONO calibration methods based on reacting NO with the HO<sub>x</sub> generated by H<sub>2</sub>O photolysis at 184.9 nm were presented. This includes a novel approach in which HONO is quantified using the  $NO_2$  formed by the  $HO_2 + NO$ reaction as a proxy. The proxy method compares well with the O<sub>3</sub> actinometry-based calibration while also having the benefit of a simpler calculation that avoids the need to characterize the emission spectrum of the mercury lamp used. In addition, this proxy method has improved uncertainties, typically between 4.5 % and 10 %  $(2\sigma)$  – lower than the  $27\% 2\sigma$  uncertainty associated with the actinometric calibration method. We also detail the potential application of a  $NO_2$  proxy calibration for  $HO_x$  calibrations, in which we anticipate exceptional  $2\sigma$  uncertainties of below 15 %. These photolytic calibrations require a direct NO<sub>2</sub> measurement, a 184.9 nm light source, and a simple quartz tube photolysis chamber. In conclusion, these photolytic calibration techniques offer a valuable alternative to the more conventional HONO calibration that is based on reacting hydrogen chloride vapor with sodium nitrite.

Data availability. The data used in this paper are available upon request.

*Supplement.* The supplement related to this article is available online at: https://doi.org/10.5194/amt-15-5455-2022-supplement.

Author contributions. AJL and ECW designed the experiments. AJL carried them out and performed the data analysis. AJL prepared the manuscript with contributions from ECW.

*Competing interests.* The contact author has declared that none of the authors has any competing interests.

*Disclaimer.* Publisher's note: Copernicus Publications remains neutral with regard to jurisdictional claims in published maps and institutional affiliations.

Acknowledgements. We are grateful to Phil Stevens (Indiana University) for characterizing the mercury lamp used for these calibrations.

*Financial support.* This research has been supported by the Directorate for Geosciences (grant no. AGS-2002928).

*Review statement.* This paper was edited by Lisa Whalley and reviewed by three anonymous referees.

#### References

- Bertram, T. H., Kimmel, J. R., Crisp, T. A., Ryder, O. S., Yatavelli, R. L. N., Thornton, J. A., Cubison, M. J., Gonin, M., and Worsnop, D. R.: A field-deployable, chemical ionization time-of-flight mass spectrometer, Atmos. Meas. Tech., 4, 1471–1479, https://doi.org/10.5194/amt-4-1471-2011, 2011.
- Bloss, W. J., Lee, J. D., Heard, D. E., Salmon, R. A., Bauguitte, S. J.-B., Roscoe, H. K., and Jones, A. E.: Observations of OH and HO<sub>2</sub> radicals in coastal Antarctica, Atmos. Chem. Phys., 7, 4171–4185, https://doi.org/10.5194/acp-7-4171-2007, 2007.
- Bottorff, B., Reidy, E., Mielke, L., Dusanter, S., and Stevens, P. S.: Development of a laser-photofragmentation laser-induced fluorescence instrument for the detection of nitrous acid and hydroxyl radicals in the atmosphere, Atmos. Meas. Tech., 14, 6039–6056, https://doi.org/10.5194/amt-14-6039-2021, 2021.
- Bourgeois, I., Peischl, J., Neuman, J. A., Brown, S. S., Allen, H. M., Campuzano-Jost, P., Coggon, M. M., DiGangi, J. P., Diskin, G. S., Gilman, J. B., Gkatzelis, G. I., Guo, H., Halliday, H. A., Hanisco, T. F., Holmes, C. D., Huey, L. G., Jimenez, J. L., Lamplugh, A. D., Lee, Y. R., Lindaas, J., Moore, R. H., Nault, B. A., Nowak, J. B., Pagonis, D., Rickly, P. S., Robinson, M. A., Rollins, A. W., Selimovic, V., St. Clair, J. M., Tanner, D., Vasquez, K. T., Veres, P. R., Warneke, C., Wennberg, P. O., Washenfelder, R. A., Wiggins, E. B., Womack, C. C., Xu, L., Zarzana, K. J., and Ryerson, T. B.: Comparison of airborne measurements of NO, NO<sub>2</sub>, HONO, NO<sub>y</sub>, and CO during FIREX-AQ, Atmos. Meas. Tech., 15, 4901–4930, https://doi.org/10.5194/amt-15-4901-2022, 2022.
- Burkholder, J., Sander, S., Abbatt, J., Barker, J., Cappa, C., Crounse, J., Dibble, T., Huie, R., Kolb, C., and Kurylo, M.: Chemical kinetics and photochemical data for use in atmospheric studies, Evaluation No. 19, JPL Publication 19–5, 583–586, Jet Propulsion Laboratory, Pasadena, http://jpldataeval.jpl.nasa.gov (last access: 19 September 2022), 2020.
- Butkovskaya, N., Kukui, A., and Le Bras, G.: HNO<sub>3</sub> Forming Channel of the HO<sub>2</sub>+NO Reaction as a Function of Pressure and Temperature in the Ranges of 72–600 Torr and 223–323 K, J. Phys. Chem. A, 111, 9047–9053, https://doi.org/10.1021/jp074117m, 2007.
- Butkovskaya, N., Rayez, M.-T., Rayez, J.-C., Kukui, A., and Le Bras, G.: Water vapor effect on the HNO<sub>3</sub> yield in the HO<sub>2</sub>+ NO reaction: experimental and theoretical evidence, J. Phys. Chem. A, 113, 11327–11342, https://doi.org/10.1021/jp811428p, 2009.
- Cheng, P., Cheng, Y., Lu, K., Su, H., Yang, Q., Zou, Y., Zhao, Y., Dong, H., Zeng, L., and Zhang, Y.: An online monitoring system for atmospheric nitrous acid (HONO) based on stripping coil and ion chromatography, J. Environ. Sci., 25, 895907, https://doi.org/10.1016/s1001-0742(12)60251-4, 2013.
- Crilley, L. R., Kramer, L. J., Ouyang, B., Duan, J., Zhang, W., Tong, S., Ge, M., Tang, K., Qin, M., Xie, P., Shaw, M. D., Lewis, A.
  C., Mehra, A., Bannan, T. J., Worrall, S. D., Priestley, M., Bacak, A., Coe, H., Allan, J., Percival, C. J., Popoola, O. A. M., Jones, R. L., and Bloss, W. J.: Intercomparison of nitrous acid (HONO) measurement techniques in a megacity (Beijing), At-

- mos. Meas. Tech., 12, 6449–6463, https://doi.org/10.5194/amt-12-6449-2019, 2019.
- Dixneuf, S., Ruth, A. A., Häseler, R., Brauers, T., Rohrer, F., and Dorn, H.-P.: Detection of nitrous acid in the atmospheric simulation chamber SAPHIR using open-path incoherent broadband cavity-enhanced absorption spectroscopy and extractive longpath absorption photometry, Atmos. Meas. Tech., 15, 945–964, https://doi.org/10.5194/amt-15-945-2022, 2022.
- Dusanter, S., Vimal, D., and Stevens, P.: Measuring tropospheric OH and HO<sub>2</sub> by laser-induced fluorescence at low pressure. A comparison of calibration techniques, Atmos. Chem. Phys., 8, 321–340, https://doi.org/10.5194/acp-8-321-2008, 2008.
- Dyson, J. E., Boustead, G. A., Fleming, L. T., Blitz, M., Stone, D., Arnold, S. R., Whalley, L. K., and Heard, D. E.: Production of HONO from NO<sub>2</sub> uptake on illuminated TiO<sub>2</sub> aerosol particles and following the illumination of mixed TiO<sub>2</sub>/ammonium nitrate particles, Atmos. Chem. Phys., 21, 5755–5775, https://doi.org/10.5194/acp-21-5755-2021, 2021.
- Faloona, I. C., Tan, D., Lesher, R. L., Hazen, N. L., Frame, C. L., Simpas, J. B., Harder, H., Martinez, M., Di Carlo, P., and Ren, X.: A laser-induced fluorescence instrument for detecting tropospheric OH and HO<sub>2</sub>: Characteristics and calibration, J. Atmos. Chem., 47, 139–167, https://doi.org/10.1023/B:JOCH.0000021036.53185.0e, 2004.
- Febo, A., Perrino, C., Gherardi, M., and Sparapani, R.: Evaluation of a high-purity and high-stability continuous generation system for nitrous acid, Environ. Sci. Technol., 29, 2390–2395, https://doi.org/10.1021/es00009a035, 1995.
- Gingerysty, N. J. and Osthoff, H. D.: A compact, high-purity source of HONO validated by Fourier transform infrared and thermal-dissociation cavity ring-down spectroscopy, Atmos. Meas. Tech., 13, 4159–4167, https://doi.org/10.5194/amt-13-4159-2020, 2020.
- Gomez Alvarez, E., Amedro, D., Afif, C., Gligorovski, S., Schoemaecker, C., Fittschen, C., Doussin, J.-F., and Wortham, H.: Unexpectedly high indoor hydroxyl radical concentrations associated with nitrous acid, P. Natl. Acad. Sci. USA, 110, 13294–13299, https://doi.org/10.1073/pnas.1308310110, 2013.
- Jaeglé, L., Shah, V., Thornton, J., Lopez-Hilfiker, F., Lee, B., McDuffie, E., Fibiger, D., Brown, S., Veres, P., and Sparks, T.: Nitrogen oxides emissions, chemistry, deposition, and export over the Northeast United States during the WINTER aircraft campaign, J. Geohys. Res.-Atmos., 123, 12368–312393, https://doi.org/10.1029/2018JD029133, 2018.
- Jiang, Y., Xue, L., Gu, R., Jia, M., Zhang, Y., Wen, L., Zheng, P., Chen, T., Li, H., Shan, Y., Zhao, Y., Guo, Z., Bi, Y., Liu, H., Ding, A., Zhang, Q., and Wang, W.: Sources of nitrous acid (HONO) in the upper boundary layer and lower free troposphere of the North China Plain: insights from the Mount Tai Observatory, Atmos. Chem. Phys., 20, 12115–12131, https://doi.org/10.5194/acp-20-12115-2020, 2020.
- Jiang, Y., Xue, L., Shen, H., Dong, C., Xiao, Z., and Wang, W.: Dominant Processes of HONO Derived from Multiple Field Observations in Contrasting Environments, Environ. Sci. Tech. Let., 9, 258–264, https://doi.org/10.1021/acs.estlett.2c00004, 2022.
- Kebabian, P. L., Wood, E. C., Herndon, S. C., and Freedman, A.: A practical alternative to chemiluminescence-based detection of nitrogen dioxide: Cavity attenuated phase

- shift spectroscopy, Environ. Sci. Technol., 42, 6040–6045, https://doi.org/10.1021/es703204j, 2008.
- Lanzendorf, E., Hanisco, T., Donahue, N., and Wennberg, P.: Comment on: "The measurement of tropospheric OH radicals by laser-induced fluorescence spectroscopy during the POP-CORN Field Campaign" by Hofzumahaus et al. and "Intercomparison of tropospheric OH radical measurements by multiple folded long-path laser absorption and laser induced fluorescence" by Brauers et al., Geophys. Res. Lett., 24, 3037–3038, https://doi.org/10.1029/97GL02899, 1997.
- Lao, M., Crilley, L. R., Salehpoor, L., Furlani, T. C., Bourgeois, I., Neuman, J. A., Rollins, A. W., Veres, P. R., Washenfelder, R. A., Womack, C. C., Young, C. J., and VandenBoer, T. C.: A portable, robust, stable, and tunable calibration source for gasphase nitrous acid (HONO), Atmos. Meas. Tech., 13, 5873–5890, https://doi.org/10.5194/amt-13-5873-2020, 2020.
- Lee, B., Wood, E., Wormhoudt, J., Shorter, J., Herndon, S., Zahniser, M., and Munger, J.: Effective line strengths of trans-nitrous acid near 1275 cm<sup>-1</sup> and cis-nitrous acid at 1660 cm<sup>-1</sup>, J. Quant. Spectrosc. Ra., 113, 1905–1912, https://doi.org/10.1016/j.jqsrt.2012.06.004, 2012.
- Lee, B. H., Lopez-Hilfiker, F. D., Mohr, C., Kurtén, T., Worsnop, D. R., and Thornton, J. A.: An iodide-adduct high-resolution time-of-flight chemical-ionization mass spectrometer: Application to atmospheric inorganic and organic compounds, Environ. Sci. Technol., 48, 6309–6317, https://doi.org/10.1021/es500362a, 2014.
- Li, X., Rohrer, F., Hofzumahaus, A., Brauers, T., Häseler, R., Bohn, B., Broch, S., Fuchs, H., Gomm, S., and Holland, F.: Missing gas-phase source of HONO inferred from Zeppelin measurements in the troposphere, Science, 344, 292–296, https://doi.org/10.1126/science.1248999, 2014.
- Lu, K., Fuchs, H., Hofzumahaus, A., Tan, Z., Wang, H., Zhang, L., Schmitt, S. H., Rohrer, F., Bohn, B., and Broch, S.: Fast photochemistry in wintertime haze: consequences for pollution mitigation strategies, Environ. Sci. Technol., 53, 10676–10684, https://doi.org/10.1021/acs.est.9b02422, 2019.
- Novak, G. A., Vermeuel, M. P., and Bertram, T. H.: Simultaneous detection of ozone and nitrogen dioxide by oxygen anion chemical ionization mass spectrometry: a fast-time-response sensor suitable for eddy covariance measurements, Atmos. Meas. Tech., 13, 1887–1907, https://doi.org/10.5194/amt-13-1887-2020, 2020.
- Peng, Q., Palm, B. B., Melander, K. E., Lee, B. H., Hall, S. R., Ullmann, K., Campos, T., Weinheimer, A. J., Apel, E. C., and Hornbrook, R. S.: HONO emissions from western US wildfires provide dominant radical source in fresh wildfire smoke, Environ. Sci. Technol., 54, 5954–5963, https://doi.org/10.1021/acs.est.0c00126, 2020.
- Pinto, J. P., Dibb, J., Lee, B. H., Rappenglück, B., Wood, E. C., Levy, M., Zhang, R. Y., Lefer, B., Ren, X. R., Stutz, J., Tsai, C., Ackermann, L., Golovko, J., Herndon, S. C., Oakes, M., Meng, Q. Y., Munger, J. W., Zahniser, M., and Zheng, J.: Intercomparison of field measurements of nitrous acid (HONO) during the SHARP campaign, J. Geophys. Res.-Atmos., 119, 5583–5601, https://doi.org/10.1002/2013jd020287, 2014.
- Ren, X., Van Duin, D., Cazorla, M., Chen, S., Mao, J., Zhang, L., Brune, W. H., Flynn, J. H., Grossberg, N., and Lefer, B. L.: Atmospheric oxidation chemistry and ozone production: Results

- from SHARP 2009 in Houston, Texas, J. Geophys. Res.-Atmos., 118, 5770–5780, https://doi.org/10.1002/jgrd.50342, 2013.
- Schultz, M., Heitlinger, M., Mihelcic, D., and Volz-Thomas, A.: Calibration source for peroxy radicals with built-in actinometry using H<sub>2</sub>O and O<sub>2</sub> photolysis at 185 nm, J. Geophys. Res.-Atmos., 100, 18811–18816, https://doi.org/10.1029/95JD01642, 1995.
- Slater, E. J., Whalley, L. K., Woodward-Massey, R., Ye, C., Lee, J. D., Squires, F., Hopkins, J. R., Dunmore, R. E., Shaw, M., Hamilton, J. F., Lewis, A. C., Crilley, L. R., Kramer, L., Bloss, W., Vu, T., Sun, Y., Xu, W., Yue, S., Ren, L., Acton, W. J. F., Hewitt, C. N., Wang, X., Fu, P., and Heard, D. E.: Elevated levels of OH observed in haze events during winter-time in central Beijing, Atmos. Chem. Phys., 20, 14847–14871, https://doi.org/10.5194/acp-20-14847-2020, 2020.
- Stevens, P., Mather, J., and Brune, W.: Measurement of tropospheric OH and HO<sub>2</sub> by laser-induced fluorescence at low pressure, J. Geophys. Res.-Atmos., 99, 3543–3557, https://doi.org/10.1029/93JD03342, 1994.
- Stutz, J., Oh, H.-J., Whitlow, S. I., Anderson, C., Dibb, J. E., Flynn, J. H., Rappenglück, B., and Lefer, B.: Simultaneous DOAS and mist-chamber IC measurements of HONO in Houston, TX, Atmos. Environ., 44, 4090–4098, https://doi.org/10.1016/j.atmosenv.2009.02.003, 2010.
- Tuite, K., Thomas, J. L., Veres, P. R., Roberts, J. M., Stevens, P. S., Griffith, S. M., Dusanter, S., Flynn, J. H., Ahmed, S., and Emmons, L.: Quantifying nitrous acid formation mechanisms using measured vertical profiles during the CalNex 2010 campaign and 1D column modeling, J. Geophys. Res.-Atmos., 126, e2021JD034689, https://doi.org/10.1029/2021JD034689, 2021.
- Veres, P. R., Roberts, J. M., Wild, R. J., Edwards, P. M., Brown, S. S., Bates, T. S., Quinn, P. K., Johnson, J. E., Zamora, R. J., and de Gouw, J.: Peroxynitric acid (HO<sub>2</sub>NO<sub>2</sub>) measurements during the UBWOS 2013 and 2014 studies using iodide ion chemical ionization mass spectrometry, Atmos. Chem. Phys., 15, 8101–8114, https://doi.org/10.5194/acp-15-8101-2015, 2015.
- Veres, P. R., Neuman, J. A., Bertram, T. H., Assaf, E., Wolfe, G. M., Williamson, C. J., Weinzierl, B., Tilmes, S., Thompson, C. R., and Thames, A. B.: Global airborne sampling reveals a previously unobserved dimethyl sulfide oxidation mechanism in the marine atmosphere, P. Natl. Acad. Sci. USA, 117, 4505–4510, https://doi.org/10.1073/pnas.1919344117, 2020.
- Villena, G. and Kleffmann, J.: A source for the continuous generation of pure and quantifiable HONO mixtures, Atmos. Meas. Tech., 15, 627–637, https://doi.org/10.5194/amt-15-627-2022, 2022.

- Villena, G., Kleffmann, J., Kurtenbach, R., Wiesen, P., Lissi, E., Rubio, M. A., Croxatto, G., and Rappenglück, B.: Vertical gradients of HONO, NO<sub>x</sub> and O<sub>3</sub> in Santiago de Chile, Atmos. Environ., 45, 3867–3873, https://doi.org/10.1016/j.atmosenv.2011.01.073, 2011.
- Wang, C., Bottorff, B., Reidy, E., Rosales, C. M. F., Collins, D. B., Novoselac, A., Farmer, D. K., Vance, M. E., Stevens, P. S., and Abbatt, J. P.: Cooking, bleach cleaning, and air conditioning strongly impact levels of HONO in a house, Environ. Sci. Technol., 54, 13488–13497, https://doi.org/10.1021/acs.est.0c05356, 2020.
- Whalley, L. K., Stone, D., Dunmore, R., Hamilton, J., Hopkins, J. R., Lee, J. D., Lewis, A. C., Williams, P., Kleffmann, J., Laufs, S., Woodward-Massey, R., and Heard, D. E.: Understanding in situ ozone production in the summertime through radical observations and modelling studies during the Clean air for London project (ClearfLo), Atmos. Chem. Phys., 18, 2547–2571, https://doi.org/10.5194/acp-18-2547-2018, 2018.
- Wong, K. W., Tsai, C., Lefer, B., Haman, C., Grossberg, N., Brune, W. H., Ren, X., Luke, W., and Stutz, J.: Daytime HONO vertical gradients during SHARP 2009 in Houston, TX, Atmos. Chem. Phys., 12, 635–652, https://doi.org/10.5194/acp-12-635-2012, 2012.
- Ye, C., Gao, H., Zhang, N., and Zhou, X.: Photolysis of Nitric Acid and Nitrate on Natural and Artificial Surfaces, Environ. Sci. Technol., 50, 3530–3536, https://doi.org/10.1021/acs.est.5b05032, 2016.
- Ye, C., Zhang, N., Gao, H., and Zhou, X.: Photolysis of Particulate Nitrate as a Source of HONO and NO<sub>x</sub>, Environ. Sci. Technol., 51, 6849–6856. https://doi.org/10.1021/acs.est.7b00387, 2017.
- York, D., Evensen, N. M., Martinez, M. L., and De Basabe Delgado, J.: Unified equations for the slope, intercept, and standard errors of the best straight line, Am. J. Phys., 72, 367–375, https://doi.org/10.1119/1.1632486, 2004.
- Young, C. J., Washenfelder, R. A., Roberts, J. M., Mielke, L. H., Osthoff, H. D., Tsai, C., Pikelnaya, O., Stutz, J., Veres, P. R., Cochran, A. K., VandenBoer, T. C., Flynn, J., Grossberg, N., Haman, C. L., Lefer, B., Stark, H., Graus, M., de Gouw, J., Gilman, J. B., Kuster, W. C., and Brown, S. S.: Vertically resolved measurements of nighttime radical reservoirs in Los Angeles and their contribution to the urban radical budget, Environ. Sci. Technol., 46, 10965–10973, https://doi.org/10.1021/es302206a, 2012.